Journal of GeoEngineering, Vol. 14, No. 4, pp. 259-276, December 2019
http://dx.doi.org/10.6310/jog.201912_14(4).5

3D NONLINEAR FINITE ELEMENT ANALYSIS OF PILED-RAFT FOUNDATION FOR TALL WIND TURBINES AND ITS COMPARISON WITH ANALYTICAL MODEL

Shweta Shrestha [1] and Nadarajah Ravichandran [2*]

ABSTRACT

Geotechnical design of piled-raft foundation is typically performed using simplified semi-empirical equations that do not consider the interaction between structural components and supporting soil and the effect of bending moment on the differential settlement of piled-raft. In this study, the settlements and rotations computed using an analytical and linear and nonlinear finite element methods were compared. First, a piled-raft foundation for supporting a 130 m-tall wind turbine was designed using simplified analytical method and then a nonlinear finite element model was created in ABAQUS and analyzed. In the finite element modeling, the stress-strain behavior of the soil was represented by linear elastic (LE) and nonlinear elastoplastic Drucker-Prager (DP) models. The interfaces between structural components and soil were modeled as two bodies in the contact that allows slipping and separation at the interfaces. The results showed that the vertical and the horizontal displacements from the analytical procedure were significantly higher than that of the nonlinear finite element method. At the same time, the differential settlement and rotation were lower than that of ABAQUS. The parametric study conducted by varying the wind speed and undrained shear strength of the soil indicates that the difference between the predicted responses decreases when the load is large and/or soil is soft. From the finite element analyses, it was observed that the separation and slip between the soil and pile were negligible. It was also found that the piles contributed more in reducing vertical settlement, raft contributed more in reducing horizontal displacement, and only piles were contributing to reduce differential settlement.

Key words: Piled-raft foundation, finite element analysis, ABAQUS, soil-pile interaction, differential settlement, Drucker-Prager.

1. INTRODUCTION

The importance of meeting the energy demand through clean and sustainable sources has been well recognized in recent years. Among the many sustainable sources, the wind is gaining popularity around the world particularly in the USA and Europe. The wind energy production can be increased either by building taller turbine towers to access steadier and higher wind speed or by building many turbines. Selection of site for building a wind farm depends on site-specific wind characteristics and subsurface condition that affects the design and construction of the foundation for supporting the wind turbines. In some areas, the wind characteristics may be favorable, but the subsurface condition may not be suitable for transferring the larger vertical load, horizontal load and moment to the subsurface soil. This will result in a larger and uneconomical foundation, especially when the foundation must support tall turbines that induce larger moment at the base of the tower.

Mat foundation, pile group foundation, and piled-raft foundation are commonly used for supporting wind turbines. Out of these three foundation types, the piled-raft foundation (shown in Fig. 2 later) that has a large mat at the top of a number of deep foundations is economical for tall onshore wind turbine, especially when the subsurface soil is weak (Shrestha and Ravichandran 2016). Higher bearing resistance is derived from the mat foundation while higher settlement resistance is derived from the deep foundation. Although the combined mat and deep foundation is better for meeting the safety and serviceability requirements effectively, the geotechnical design of piled-raft foundation is complicated because of the complex load transfer and soil-structure interaction mechanisms. The load sharing between the piles and raft are not well understood especially when the piled-raft is for supporting wind turbine that induces shear and moment loads in addition to the vertical load. There are a few analytical methods available for the design of piled-raft foundation in the literature (Poulos and Davis 1980; Poulos 2001; Randolph 1994; Burland 1995; Hemsley 2000). The details of these methods are given in the analytical design section.

Although these simplified methods can be used to perform designs to a reasonable extent for certain geometric and loading conditions, the literature still lacks a reliable method that considers the complex load transfer and interaction mechanisms accurately. In such situations, a numerical method can be used for gaining insights into the behavior of piled-raft foundation subjected to complex loading conditions. With the rapid advancement in computer technology and efficient algorithm development for accurately representing the interaction between contacting surfaces, computer models of piled-raft foundation can be developed and analyzed within a reasonable time. Ruel and Randolph (2003) presented a comparative study of a 3D finite

Manuscript received January 30, 2019; revised May 20, 2019; accepted July 15, 2019.
[1] Graduate Student, Glenn Department of Civil Engineering, Clemson University, 123 Lowry Hall, Clemson, SC 29634, U.S.A..
[2*] Associate Professor (corresponding author), Glenn Department of Civil Engineering, Clemson University, 202A Lowry Hall, Clemson, SC 29634, U.S.A. (e-mail: nravic@clemson.edu).

element analysis (FEA) results of three instrumented piled-raft foundations by implementing ABAQUS. They found a reasonable agreement of the overall settlement and differential settlement obtained from the FEA and in-situ measurements for all three foundations. However, the proportion of the total load carried by piles obtained from finite element (FE) results was higher than that obtained from the in-situ measurements. But only 15% of the piles being instrumented, it is questionable if all the piles will behave in the same way. Lee *et al*. (2009) studied the bearing behavior of piled-raft foundation on soft clay under vertical loading by developing a 3D FE model using ABAQUS. In their study, the pile-soil interface slip was allowed, and the length of pile, number of piles, pile configuration, and load on the raft were varied to study the effects of pile-soil slip. They concluded that the slip analysis resulted in the higher average settlement and the lower maximum pile loads compared to no slip analysis. Sinha and Hanna (2016) developed a 3D model of a piled-raft foundation considering the pile-soil-raft interaction to examine the effect of the parameters such as foundation geometry, pile length, pile size, pile spacing, pile diameter, raft thickness, cohesion, and friction angle on the settlements (center, corner, and differential settlements) of the foundation under vertical loading. They concluded that the pile shape has the negligible effect on the settlements while the increase in the pile spacing resulted in the increase in settlements. On the other hand, the increase in pile length, friction angle, and cohesion of soil resulted in the decrease in settlements. Similarly, the use of a thicker raft minimized the differential settlement but at the same time imposed an additional load on some of the piles leading to ununiform settlement of the raft.

The aforementioned methods accounted for the pile-soil-raft interaction by using the interaction property or using the rough contact but did not consider the effect of bending moment on the differential settlement. For the tall structures, the design approach should also consider the bending moment as it is the major factor contributing to the differential settlement of the foundation. Moreover, either a rectangular or square raft is considered with the pile configuration in a grid pattern in the previous studies. This study presents the development of a three-dimensional (3D) FE model of the piled-raft foundation in ABAQUS by accounting for the pile-soil interaction and the combined loading (vertical load, horizontal load, and bending moment). The raft considered in this study is circular which is appropriate for a wind turbine tower, and the piles are arranged in a circular pattern. Two constitutive models were used to represent the stress-strain behavior of the soil: linear elastic (LE) and nonlinear elastoplastic Drucker-Prager (DP) models. The objectives of this study are to: (i) perform the analytical design of the piled-raft foundation, (ii) conduct the finite element analysis of the piled-raft foundation using LE and DP constitutive models for soil, (iii) compare the analytical design results with the finite element analysis results, (iv) conduct a parametric study by varying the wind speed and the undrained cohesion in order to investigate the effect on the response, and (iv) investigate the results from FEA to obtain the useful information which may not be possible to obtain from the experiments.

2. CURRENT DESIGN PROCEDURES

In theory, the piled-raft foundation is economical and shows better performance compared to conventional raft or pile group foundation for supporting larger combined loads. The principal working theory of the piled-raft foundation is that the raft provides significant bearing resistance and the piles provide significant settlement resistance. Hence, the combined pile-raft system provides superior bearing and settlement resistance. Although reasonably accurate equations and procedures are available for the geotechnical design of raft and single pile or group of piles, only a few simplified procedures are available to design piled-raft foundation in the literature. This is mainly due to the lack of understanding of the 3D complex pile-soil-raft interaction that greatly influences the load sharing between the raft and piles. The major challenge during the design of piled-raft foundation is the quantification of load shared by the raft and piles and the mobilized strength of each component, all of which depends on pile-soil-raft interaction. The challenges in designing the piled-raft foundation further increase when it is subjected to the combined vertical load, horizontal load, and bending moment. As a result, reliable design guidelines are not yet available to design piled-raft foundations.

The methods available in the literature to design piled-raft foundation are broadly classified into three categories: simplified methods, approximate methods, and more rigorous computer-based methods (Deka 2014). The simplified method of analyzing a piled-raft foundation includes the analytical equations based on the elastic theory proposed by Poulos and Davis (1980), Poulos (2001), Randolph (1994), Burland (1995), and Hemsley (2000). The approximate method is based on the strip on spring or plate on spring where the raft is represented either by plate or strip and piles are represented by spring. The rigorous computer-based methods include the use of numerical solution using the commercially available software based on the finite element, finite difference, and boundary element methods. With the rapid development of computer technologies over the past few decades, a 3D finite element method has gained popularity among the designers to solve the complex piled-raft problem.

In this study, the settlement response of piled-raft foundation for supporting a tall wind turbine predicted by the simplified method and linear and nonlinear finite element methods were compared to investigate the relative accuracy of the models. The finite element model was then used to gain further insights into the behavior of piles-raft-soil system such as load sharing between piles and raft, slip and separation at the pile-soil interface and the deformation behavior of soil and pile.

3. DESIGN LOADS AND SOIL PROPERTIES

The piled-raft foundation in this study was designed for a 130 m tall hybrid wind turbine tower made of lower 93 m of concrete and upper 37 m of steel. The wind turbine specifications (diameter, height, and material) were obtained from Grunbeg and Gohlmann (2013). It was assumed that the wind turbine is to be constructed at a hypothetical site with a clayey soil deposit. During the operation of the wind turbine, the foundation will be subjected to vertical load due to self-weight of the superstructure and turbine components, horizontal load due to wind action on the components above the ground, and bending moment induced by the horizontal wind load. The calculation of each load and the soil properties for the analytical and FE modeling are discussed below.

3.1 Design Loads

The piled-raft foundation will be subjected to the vertical load due to the weight of the tower and other turbine components and the horizontal load and bending moment due to the wind acting on the tower body. The vertical load was calculated by adding the weights of the tower and other components of the wind turbine such as nacelle and rotor. The weight of the tower was calculated using the tower dimension and corresponding unit weights of the tower components and the weights of nacelle and rotor were obtained from Malhotra (2011). The final dead load was calculated to be 51.71 MN.

The wind action on the structures above the ground induces horizontal load on them which results in a horizontal load and bending moment at the base of the tower. The wind load was calculated following the procedure described in ASCE 7-10 (2010) using the mean survival wind speed of 201.3 km/h. This mean wind speed is considered to be appropriate because most of the wind turbines have the survival wind speed within 180.3 km/h to 215.7 km/h (Wagner and Mathur 2013) and its range lies between 143.3 km/h and 259.2 km/h. The total horizontal load and bending moment were calculated to be 2.26 MN and 144.89 MNm, respectively. It should be noted that a parametric study was conducted by varying the wind speed for comparing the predictions for a wide range of horizontal load and bending moment.

3.2 Soil Properties

A site composed of a single layer of clayey soil was considered in this study. The unit weight and mean undrained cohesion for the clayey soil were assumed to be 18 kN/m^3 and 100 kN/m^2, respectively. The modulus of elasticity of the soil was determined using the correlation between undrained cohesion and modulus of elasticity obtained from USACE (1990) and was calculated to be 3.5×10^4 kN/m^2. The determination of the nonlinear elastoplastic constitutive model parameters is described in the finite element modeling section. A parametric study was also conducted by varying the undrained cohesion and corresponding modulus of elasticity to investigate the effect of soil properties on the predicted performance.

4. DESIGN OF PILED-RAFT FOUNDATION USING ANALYTICAL METHOD

The geotechnical design of the piled-raft foundation (determination of dimensions of raft, type of piles, dimensions of piles, number of piles, and arrangement of piles) was conducted using the simplified approach proposed by Hemsley (2000) in which the design procedures proposed by Poulos and Davis (1980) and Randolph (1994) are incorporated. In addition, a new iterative procedure was developed to calculate the differential settlement of the piled raft foundation due to the bending moment. At first, the radius of the raft, the length of the piles, the number of piles, and arrangement of the piles were assumed and adjusted until all the design requirements were met. The design requirements include stability checks (vertical load capacity, horizontal load capacity, and bending moment capacity) and serviceability checks (total and differential settlements, and the rotation of the tower per unit length). A minimum factor of safety of 2.0 was considered to be safe (Hemsley 2000) for vertical load, horizontal load, and bending moment capacity checks. A vertical misalignment within 3 mm/m of the tower was considered to be safe against the rotation of the tower which yielded the allowable rotation and differential settlement of 0.172° and 45 mm (Grunberg and Gohlmann 2013) for the problem considered in this study.

4.1 Stability Check

4.1.1 Vertical Load Capacity

The vertical load capacity of the piled-raft is the smaller of: (i) the sum of ultimate capacities of the raft and all the piles and (ii) the ultimate capacity of the piled-raft system as a single block. For case (i), the ultimate bearing capacity of the raft was calculated using the general bearing capacity equation and that of piles was calculated using the α-method for clayey soil. For case (ii), the ultimate capacity of the block was calculated as the ultimate capacity of the block that consists of raft, piles, portion of the raft outside the periphery of the piles and the soil. For the soil properties and loading considered in this study, the final design was controlled by the individual component failure (either raft or piles fail) that is the case (i). The vertical load capacity determined using this procedure was then compared with the design vertical load. The calculated factor of safety was determined to be 4.06, which meets the design requirement.

4.1.2 Moment Capacity

The moment capacity of the piled-raft foundation was calculated following a similar procedure used for calculating the vertical load capacity. The moment capacity of the individual components and the block was first determined using the method presented in Hemsley (2000). Then, the moment capacity of the piled-raft foundation was determined as the smaller of: (i) the ultimate moment capacity of the raft and the individual piles and (ii) the ultimate moment capacity of the piled-raft foundation as a single block. Based on the calculations it was found that the design was controlled by individual component failure and the resulting factor of safety was 4.23 that meets the design requirement.

4.1.3 Horizontal Load Capacity

The horizontal capacity of the piled-raft foundation was estimated following Broms' solution outlined in Gudmundsdottir (1981) for the lateral pile analysis in cohesive soil. Although this method is for single pile analysis, it was assumed that all the piles in the group will have similar behavior. The horizontal coefficient of subgrade reaction was used to determine the horizontal load capacity and horizontal deflection of the pile. The horizontal load capacity of the piled-raft was compared with the design horizontal load and the factor of safety was found to be 14.23 and the horizontal deflection was found to be 7.10 mm.

4.2 Serviceability Check

4.2.1 Vertical Settlement of the Piled-Raft

The vertical load-settlement behavior of the piled-raft was estimated by the approach proposed by Poulos (2001) in con-

junction with the method used for estimating the load sharing between the raft and the piles presented in Randolph (1994). The stiffness of the piles, raft, and pile-raft as a single block was used to estimate the load sharing between the raft and the piles. The stiffness of the piled-raft, K_{pr}, was estimated using Eq. (1) proposed by Randolph (1994).

$$K_{pr} = X K_p \; ; \; X = \frac{1+(1-2\alpha_{rp})K_r/K_p}{1-\alpha_{rp}^2(K_r/K_p)} \tag{1}$$

where K_r is the stiffness of raft, K_p is the stiffness of the pile group, and α_{rp} is the pile-raft interaction factor. The pile-raft interaction factor was assumed to be 0.8 considering the fact that when the number of piles in the group increases the value of the interaction factor increases and it reaches a constant value of 0.8 as reported by Clancy and Randolph (1993). The stiffness of the raft was estimated using the method outlined by Randolph (1994) and the stiffness of the pile group was estimated using the method proposed by Poulos (2001). In this method, the target stiffness of the piled-raft was first determined by dividing the total vertical load by the assumed allowable settlement and then the Eq. (1) was solved to determine the stiffness of the pile group.

To introduce the effect of inelastic behavior of soil, it was assumed that the load-settlement relationship is hyperbolic in nature. Hence the stiffness of piles and raft were replaced by secant stiffness using the hyperbolic factors shown in Eq. (2).

$$K_p = K_{pi}\left(1-\frac{R_{fp}P_p}{P_{pu}}\right) \; ; \; K_r = K_{ri}\left(1-\frac{R_{fr}P_r}{P_{ru}}\right) \tag{2}$$

where K_{pi} and K_{ri} is the initial stiffnesses of pile group and raft, respectively. R_{fp} and R_{fr} are the hyperbolic factors for piles and raft, respectively. P_p and P_r are the loads carried by piles and raft, respectively. P_{pu} and P_{ru} are the ultimate capacities of the piles and raft, respectively. In this study, the hyperbolic factors of 0.5 and 0.75 were used for piles and raft, respectively as suggested by Hemsley (2000). When the foundation is subjected to the vertical load, the stiffness of the piled-raft will remain operative until the load-bearing capacity of the pile is fully mobilized at load P_A as shown in Eq. (3) (also in Fig. 1). After calculating the values of K_p, K_r, K_{pr}, and P_A, the load-settlement curve (P *vs.* S) for the piled-raft foundation was developed using the Eq. (3) and the resultant vertical load-settlement curve is shown in Fig. 1.

$$\text{For } P \le P_A \; ; \; S = \frac{P}{K_{pr}}$$

$$\text{For } P > P_A \; ; \; S = \frac{P_A}{K_{pr}} + \frac{P-P_A}{K_r} \tag{3}$$

From the above load-settlement curve, it was determined that the piled-raft foundation considered in this study would settle vertically by 41.90 mm when subjected to the design vertical load of 51.71 MN. It should also be noted that the design vertical load is smaller than P_A (= 227.04 MN) which indicates that both the raft and the piles are contributing to support the load and the piles capacity is not fully mobilized at this vertical load.

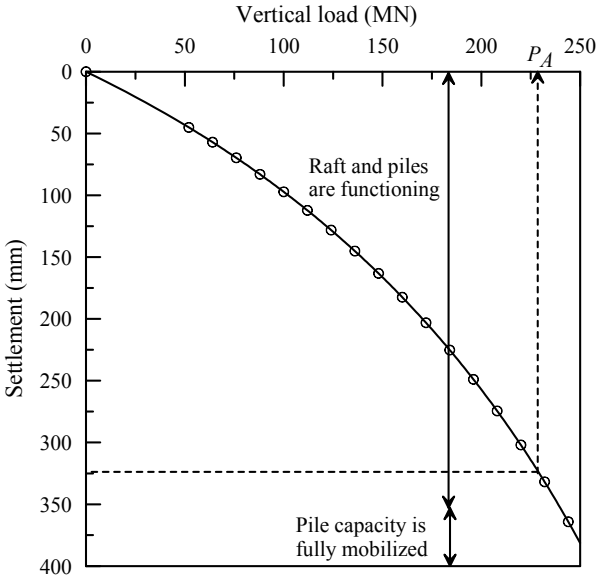

Fig.1 Load-settlement curve for the piled-raft foundation based on the analytical model

4.2.2 Differential Settlement and Rotation of the Piled-Raft

The calculation of differential settlement of the combined piled-raft foundation system due to the bending moment is another challenging task in the geotechnical design of piled-raft foundation. The accurate procedure to estimate the differential settlement due to bending moment is not yet available in the literature. This paper proposes a new method to calculate the differential settlement of the piled-raft foundation due to the bending moment. In this method, the total applied bending moment was converted into vertical forces (their magnitude varies with distance to the pile from the center) and divided between the raft and the piles such that the differential settlements of the individual components (*i.e.*, raft and piles) were equal, which was considered as the differential settlement of the piled-raft foundation. The calculation of the differential settlement of individual components (raft and piles) is discussed in the following section.

(1) Differential settlement of raft

The differential settlement of the raft was estimated based on the rotation (θ). The rotation was calculated using Eq. (4) given by Grunberg and Gohlmann (2013).

$$\theta = \frac{M_{found}}{c_s I_{found}} \; ; \; c_s = \frac{E_s}{f'\sqrt{A_{found}}} \tag{4}$$

where M_{found} is the fixed-end moment at soil-structure interface (percentage of moment shared by raft to result in an equal differential settlement as that of piles in this study), c_s is the foundation modulus, I_{found} is the second moment of inertia for area of foundation, E_s is the modulus of elasticity of soil, f' is the shape factor for overturning (0.25), and A_{found} is the area of the foundation. After calculating θ, the differential settlement of the raft was determined using simple trigonometric relationship.

(2) Differential settlement of piles

The differential settlement profile of the piles as a group was estimated considering the equivalent vertical loads due to the dead load and bending moment shared by the piles. First, the vertical load on each pile was estimated and then the settlement of each pile head was calculated following the procedure outlined by Fellenius (1999). Finally, the settlements of the piles in a vertical section (2D elevation) were approximated by a straight line to produce the settlement profile for the piles. The above-mentioned procedure was repeated by adjusting the bending moment shared by the piles and the raft until the settlement profiles of raft and piles matched. The final settlement profile is considered as the settlement profile of the piled-raft system. After several iterations, it was found that the raft takes 12.46% and piles take 87.54% of the total bending moment to yield an equal differential settlement. The differential settlement of the piled-raft system was found to be 10.55 mm which gives a rotation of 0.04°. For the 130 m tower height, this rotation of 0.04° induces a horizontal displacement of 91.41 mm at the top of the tower which is within the acceptable limit.

The final design that meets all the geotechnical design requirements (safety and serviceability) resulted in a raft of radius of 7.5 m and thickness 1.2 m at a depth of 1.5 m supported by 44 pre-stressed concrete piles of width 0.457 m and length 28.0 m arranged equally along the circumferences with radii of 5.3 m and 6.7 m. The final design is shown in Fig. 2.

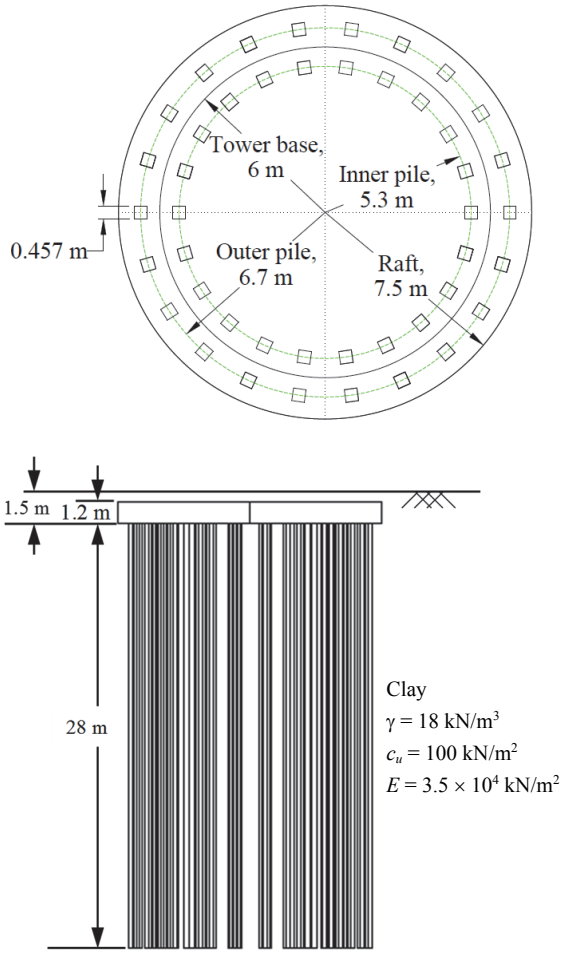

Fig. 2 Plan and elevation of designed piled-raft foundation

5. ANALYSIS OF PILED-RAFT FOUNDATION USING COUPLED FINITE ELEMENT METHOD

5.1 Finite Element Model Development and Boundary Conditions

A 3D finite element model of the piled-raft foundation system including the supporting soil was developed using ABAQUS 6.14, a general-purpose finite element software widely used in Civil and Mechanical Engineering fields. The ability to incorporate the interaction among piles, raft, and soil is one of the key advantages of the finite element modeling over the analytical method. The dimensions of the piled-raft foundation (size of the raft, size of the piles, and location of the piles) obtained from the analytical design were used to develop its FE model in ABAQUS. First, 3D models of each of the components of the piled-raft foundation were created and spatially discretized using 8-nodehexahedral brick elements. For the supporting soil, the diameter and the height of the simulation domain was determined to be 50 m and 56 m, respectively, based on an initial size sensitivity study. The purpose of the size sensitivity study was to ensure that the simulation domain size and its boundaries do not affect the computed responses. The individual components were then assembled at their respective locations in the assembly module ensuring that the parts of the soil to be occupied by the raft and piles are removed. The assembled model is shown in Fig. 3. In the analytical design, a 1.2 m thick raft is positioned at the depth of 1.5 m from the ground surface which implies that there will be a 0.3 m thick soil above the raft. However, in Fig. 3, the soil above the raft cannot be seen because it was not modeled as a soil body. Instead, it was modeled as a uniform vertical pressure equivalent to the weight of the 0.3 m thick soil which was later applied to the model before applying the vertical and lateral loads. This was done to reduce/eliminate the numerical instabilities that may occur near the surface during the numerical analysis.

The bottom of the simulation domain was fixed in all directions, *i.e.,* no translation in x, y, and z directions. The vertical sides of the simulation domain were fixed in x and y directions (*i.e.*, in the lateral direction) and allowed to move freely in z direction (vertical direction). The top of the simulation domain was free. Figure 3 shows these boundary conditions in addition to various parts and dimensions of the simulation domain.

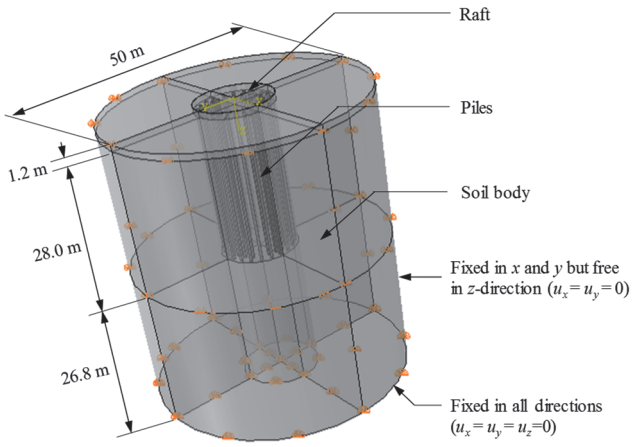

Fig. 3 Three-dimensional view of the piled-raft system in ABAQUS

5.2 Constitutive Models for the Soil and Structural Components

The mathematical representation of the stress-strain behavior of the soil and the structural elements is critical for accurately predicting the response of the piled-raft systems using finite element method. The selection of the material model depends on the expected and/or observed behavior of each component for a given load range and material properties. In general, a geotechnical system may show nonlinear elastoplastic behavior at higher load and/or lower material stiffness (*i.e.*, the system undergoes large strain). On the other hand, the same system may show linear behavior at smaller loads and/or higher material stiffness (*i.e.*, the system undergoes small strain). The linear elastic relationships are simple, computationally efficient, numerically stable, and determination of their model parameters are straight forward. On the other hand, the nonlinear elastoplastic relationships are complex, computationally expensive, numerically unstable, and determination of their model parameters requires significant effort with advanced laboratory tests. In this study, the structural components, *i.e.*, raft and piles were represented by an in-built linear elastic constitutive model because in most of the structural designs the structural components are only allowed to behave in the linear elastic range. The properties of the raft and piles are listed in Table 1.

Table 1 Structural components model parameters

Component	Density (kg/m^3)	Young's modulus (kN/m^2)	Poisson's ratio
Pile	2549.3	3.00×10^7	0.15
Raft	2549.3	3.28×10^7	0.15

The supporting soil was represented by two constitutive models: linear elastic (LE) and elastoplastic Drucker-Prager (DP) models to compare the predicted results. The purpose of using LE model to represent the soil in this study was to compare the results of the finite element simulation with the results of analytical design. Since the analytical design procedure is based on the elastic theory, the use of LE model in FEA will enable us for appropriate comparison. Since soil exhibits nonlinear elastoplastic behavior at larger deformation range, an elastoplastic DP model was also used in this study to accurately represent the stress-strain relationship of the soil and to compare the predictions with that of LE and analytical models. The use of DP model can produce realistic result compared to the linear elastic-perfectly plastic Mohr-Coulomb (MC) and LE models for large loads because it can model the modulus reduction with increasing strain. Since the experimental stress-strain relationship was not available, the DP model parameters were calibrated using the basic geotechnical strength and deformation parameters to ensure that the elastoplastic model parameters are consistent with that of linear elastic models. It should be noted that one may use laboratory test results such as triaxial test results to accurately calibrate the elastoplastic DP model parameters.

First, the linear elastic-perfectly plastic MC stress-strain relationship was developed in EXCEL using the initial elastic modulus and shear strength parameters that define the yielding. Then, the DP stress-strain relationship was formulated by using the hyperbolic relationship between the vertical strain and deviatoric stress. The calibrated stress-strain curves for the MC and DP models are shown in Fig. 4(a). The use of the DP model in ABAQUS requires the hardening model, *i.e.,* yield stress *vs.* plastic strain curve as one of the inputs. To obtain the yield stress *vs.* plastic strain curve, first, the initial yield stress was estimated as the deviator stress at which the stress-strain curve starts to exhibit nonlinear behavior. From Fig. 4(a), the initial yield stress is found to be 30 kN/m^2. Then, the plastic strains for corresponding stresses were calculated by subtracting elastic strain from the total strain. The elastic strain at each stress was calculated by dividing the stress by the initial elastic modulus. The final DP hardening curve obtained through this procedure is shown in Fig. 4(b). The other constitutive model parameters for both the LE and DP models are listed in Table 2.

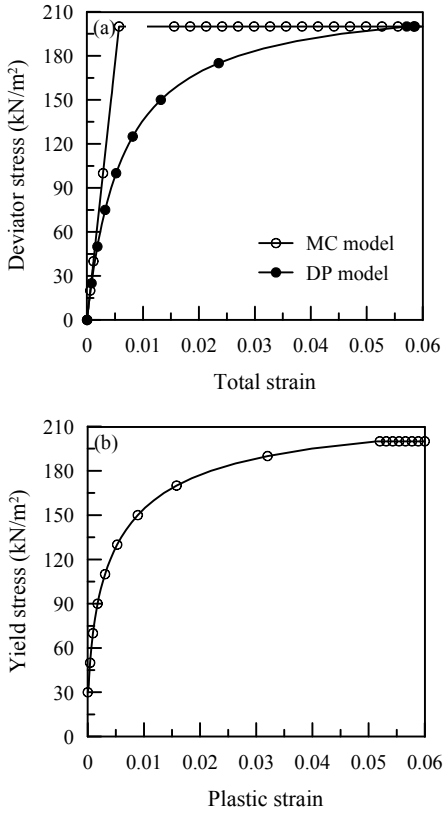

Fig. 4 (a) Calibrated MC and DP models and (b) DP hardening model inputs

Table 2 Constitutive model parameters for linear elastic and Drucker-Prager models

Model	Parameter	Value
Linear elastic	Density (kg/m^3)	1835.5
	Young's modulus (kN/m^2)	3.50×10^7
	Poisson's ratio	0.45
Drucker-Prager	Shear criterion	Linear
	Flow potential eccentricity	0.1
	Friction angle (°)	0
	Flow stress ratio	1
	Dilation angle (°)	0
	Yield stress vs plastic strain	Graphically shown in Fig. 4(b)

5.3 Spatial Discretization and Simulation Domain

The simulation domain was discretized using the linear 8-noded hexahedral brick element (C3D8R) with reduced integration and hourglass control for all the components. While generating the mesh, the nodes at the interface between contacting surfaces must coincide or be within allowable distance. To achieve this, partition technique was used to divide the components into pieces as shown in Fig. 5. An equal number of elements were assigned to the overlapping surfaces. A finer mesh was created in the areas where higher stress and/or deformation gradient was expected such as in the raft and along the soil-pile region. A coarser mesh was created in the areas where the stress concentration was expected to be lower such as the soil towards the sides and bottom.. The partition of the model and the finite element mesh generated with the internal mesh view are shown in Fig. 5. The final finite element mesh consisted of 370,979 nodes and 288,360 3D brick elements.

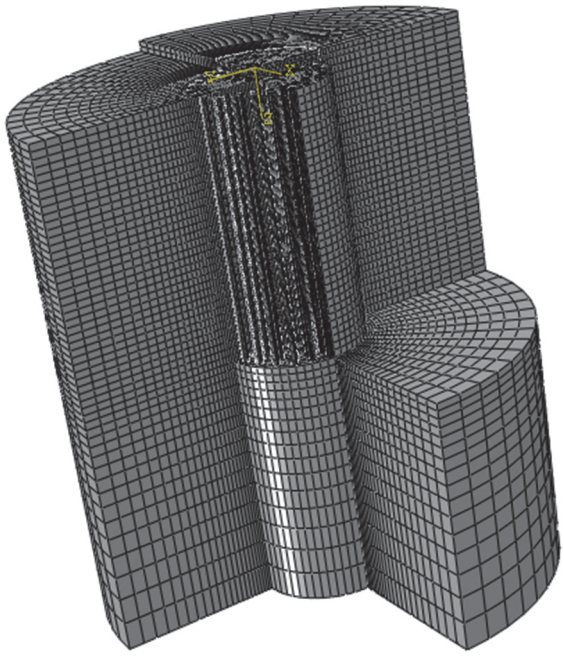

Fig. 5 Mesh (with internal mesh view)

5.4 Soil-Structure Interface Modeling

Three interfaces exist in piled-raft foundation. They are: raft-pile interface, raft-soil interface, and pile-soil interface. The external loads are first taken by the raft and then the raft transfers the loads to the piles through the raft-pile interface and to the soil through the raft-soil interface. The loads transferred to the piles are then transferred to the soil through the pile-soil interface. The accurate modeling of these interfaces is critical in the modeling of piled-raft foundation for a realistic prediction of its overall behavior.

In this study, soil-structure (raft-soil and pile-soil) and structure-structure (raft-pile) interfaces were modeled using a surface to surface contact which is used to define contact between two deformable surfaces or between a deformable surface and a rigid surface. This method uses a master-slave concept in which one of the contacting surfaces is defined as master surface and the other as slave surface. The general rule of selecting master and slave surfaces is to define the surface with coarser mesh as master surface and the one with finer mesh as slave surface or to use the stiffer body as the master surface. Also, while defining the contact constraint with the master-slave concept, the master surface can penetrate the slave surface, while the slave surface cannot penetrate the master surface. While defining the soil-structure interfaces, *i.e.*, raft-soil and pile-soil soil surface was defined as the slave surface and raft (side and bottom) and pile (skin and tip) surface was defined as the master surface. The interaction between raft-soil and pile (skin)-soil contact pairs was defined using mechanical contact in which normal and tangential behavior of the contacting surface can be defined. The interaction between pile (tip)-soil was defined using tie constraint in which two surfaces are in contact throughout the simulation and makes the translation and rotation motion equal for surfaces in contact.. The normal behavior dictates the load transfer in the normal direction and the tangential behavior dictates the load transfer in tangential direction when there is relative motion. Since the load can transfer in the normal direction only when the two surfaces are in contact, "hard" contact was used to define the normal behavior. It ensures that the surfaces are always in contact and the loads are always transferred during the simulation. The tangential behavior was defined by using "penalty" friction formulation which allows some relative motion or elastic slip of the contacting surfaces. It follows Coulomb's friction model, according to which two contacting surfaces can tolerate shear stress up to critical shear stress (τ_{crit}) within which the contacting surfaces stick to each other. Once the shear stress exceeds the critical shear stress, the sliding of the surfaces begins. As per Coulomb's friction model, the critical shear stress is defined as, $\tau_{crit} = \mu p$, where μ is defined as the coefficient of friction and p is the contact pressure. In this study, the coefficient of friction of 0.48 was used which is common in clay-structure interaction problem. Further, a critical shear displacement or an allowable elastic slip of 5 mm was defined which is a default value in ABAQUS. This allows relative motion of the surface, but it is still computationally efficient and provides accurate results (Jozefiak *et al*. 2015).

The structure-structure interface in the piled-raft foundation, *i.e.*, raft-pile interface was defined using tie constraint in which raft (bottom) surface was defined as the master surface and pile (head) surface was defined as the slave surface.

5.5 Key Steps of the Simulation

The analysis was carried out in three steps: initial step, geostatic step, and loading step. The water table was not considered in this study. The initial step is the default step in ABAQUS which is created automatically. In the initial step, the boundary conditions, interactions, and constraints are already activated which are propagated into the next step. The geostatic step establishes the equilibrium of gravitational loads and forces and verifies the initial stresses. Since the water table is not considered in this study and the saturated unit weight of the soil is used, the initial stresses calculated are the total stresses. A uniformly distributed load representing the soil mass above the raft was also applied in this step. The last step is the loading step where the design loads (vertical load, horizontal load, and bending moment) were applied in the desired directions and locations. At first, the vertical load was applied at the center node of raft without ap-

plying the horizontal load and bending moment. Then the vertical load was kept constant and the horizontal load and bending moment were applied. To transfer the bending moment applied on the raft, an MPC beam constraint was applied between center node (on the top surface) and top nodes of the raft which ties the center node with all the nodes on the top surface. All the loads were applied in time steps. In LE model, a larger time step of 0.1 was used because there is no failure due to which there will not be numerical instability. However, for DP model, smaller time steps of 0.001 and 0.0001 were used as there can be numerical instability due to a larger increment of load. After successfully developing a 3D model of the piled-raft foundation, a job was created and submitted for the analysis in Palmetto cluster which is Clemson University's high-performance computing resource. It was found that the difference in the results with the time step of 0.001 and 0.0001 was within 1%; however, the difference in wall clock time was almost six hours. Therefore, the model with the time step of 0.001 was selected for DP model in this study.

5.6 Results and Discussions

The vertical and differential settlements, horizontal displacement, and rotation of the piled-raft foundation are the key results obtained from the finite element simulation. The deformed shape of the piled-raft foundation obtained with nonlinear elastoplastic DP soil model showing vertical displacement contours at the end of loading is shown in Fig. 6. The deformation scale factor used for the deformed shape in Fig. 6 is 150 and the legend is for the vertical displacement (U3) in meter. A similar deformed shape was obtained for the piled-raft model with LE soil model which is not shown here. Due to the combined vertical load, bending moment, and horizontal load, the piled-raft foundation is settling down as well as rotating in the vertical plane of the application of the loads. The rotation in the pile can also be observed near the pile head which is the expected behavior of the pile under a bending moment. It can be seen in Fig. 6 that the displacement is the highest at the compression side and lowest at the tension side of the foundation. A gradual increase in the vertical settlement can be seen from the tension side to the compression side.

5.6.1 Settlement Response Due to Vertical Load

The vertical load-settlement curves for the piled-raft foundation with linear elastic (LE) and nonlinear elastoplastic DP soil models obtained by applying the vertical load are shown in Fig. 7. The vertical load-settlement curves shown in Fig. 7 are only for the vertical load before the application of bending moment and horizontal load. It can be observed in Fig. 7 that up to the vertical load of about 30 MN both LE and DP soil models are exhibiting linear load-settlement behavior. Beyond that, the LE soil model continues to show the linear behavior while the DP soil model displays a nonlinear behavior due to the reduction in soil modulus with increasing strain. At the design vertical load, *i.e.*, at 51.71 MN, a uniform vertical settlement of 22.67 mm was observed on the raft surface when the LE soil model was used while this value was 25.44 mm when the nonlinear elastoplastic DP soil model was used. The difference between the vertical settlements due to the LE and DP models is found to be 2.77 mm at the vertical load of 51.71 MN. However, this difference will not be the same for other vertical loads due to the nonlinear load-settlement curve for the DP soil model.

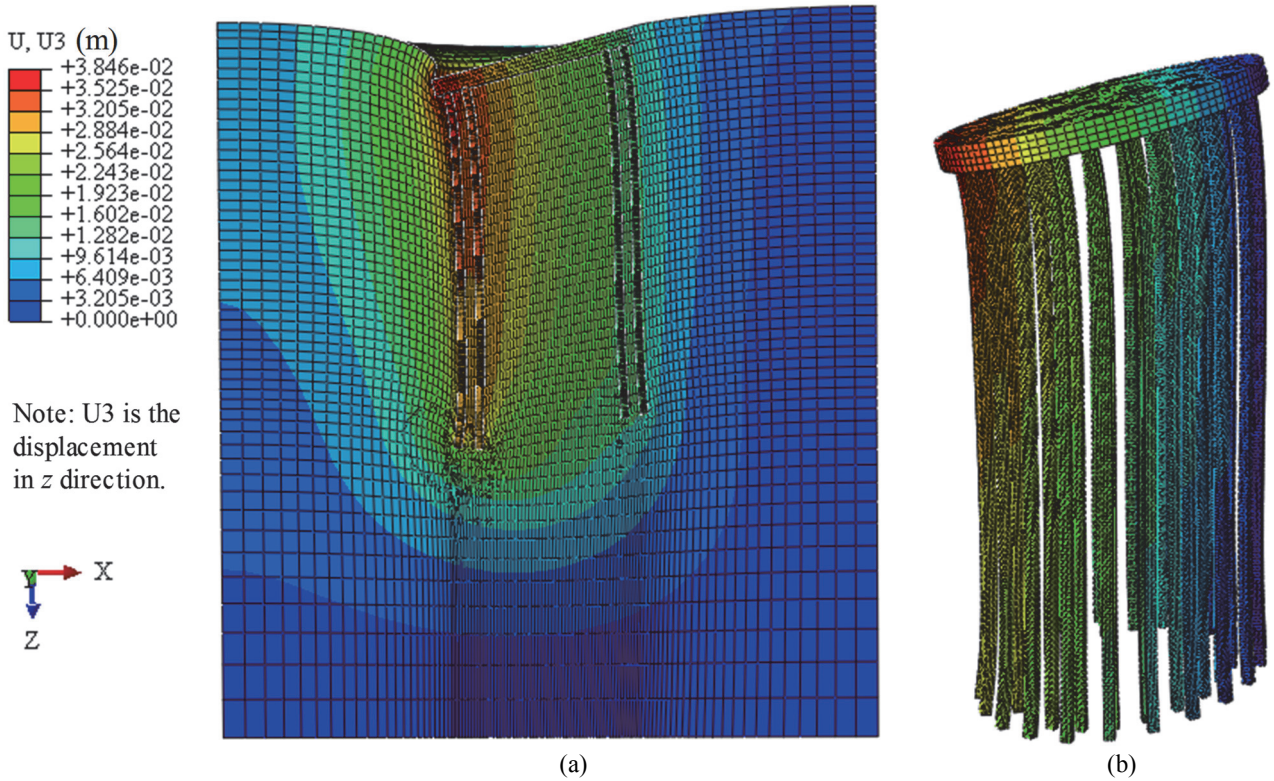

Fig. 6 Deformed shape with vertical deformation contours using DP soil model (a) cross section of the model domain and (b) piled-raft only (deformation scale factor = 150)

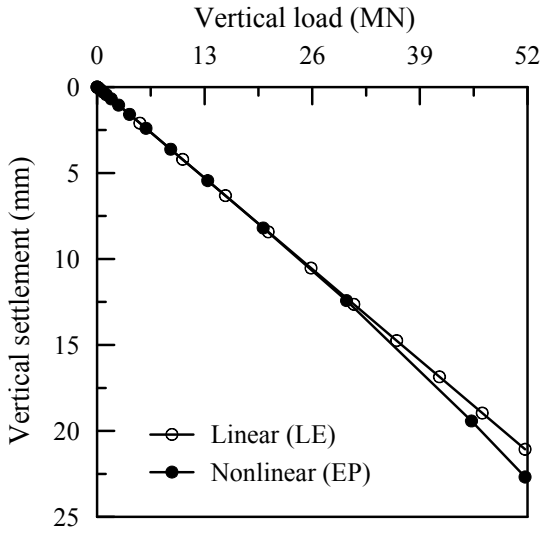

Fig. 7 Vertical settlement response of the piled-raft foundation from ABAQUS

5.6.2 Settlement and Rotation Responses Due to Bending Moment and Horizontal Load

The bending moment and horizontal load were applied at the end of the vertical load. While applying the bending moment and horizontal load, the vertical load was kept constant at its design value. The horizontal displacement, differential settlement, and rotation responses of the piled-raft foundation with the LE and DP soil models for different bending moments and horizontal loads are shown in Fig. 8(a) and 8(b). The horizontal displacement was obtained as the displacement of the raft in the direction of horizontal load (*x*-direction in this study) while the differential settlement was calculated as the difference between the vertical settlements at the extreme ends of the raft. The rotation was calculated using the differential settlement and dimension of the raft. Similar to the vertical settlement response, for the LE soil model, a linearly increasing trend of the horizontal displacement, differential settlement, and rotation were observed with increasing load. While for the DP soil model, a nonlinear settlement and rotation responses were observed. For all the loads, the DP model resulted in higher settlement and rotation compared to the LE model. At the end, the loading, the piled-raft model with the LE soil model resulted in a horizontal displacement of 5.64 mm, differential settlement of 23.05 mm, and the rotation of 0.18°. On the other hand, the piled-raft model with the DP soil model resulted in a horizontal displacement of 7.29 mm, differential settlement of 26.00 mm, and the rotation of 0.20°. The difference between the horizontal displacement due to the LE and DP model at the design horizontal load of 2.26 MN is found to be 1.65 mm and the difference in the differential settlement at the design bending moment of 144.89 MN·m is found to be 2.95 mm. Similar to the case of the vertical load-settlement curve, this difference will not be the same for other loads due to nonlinear DP model.

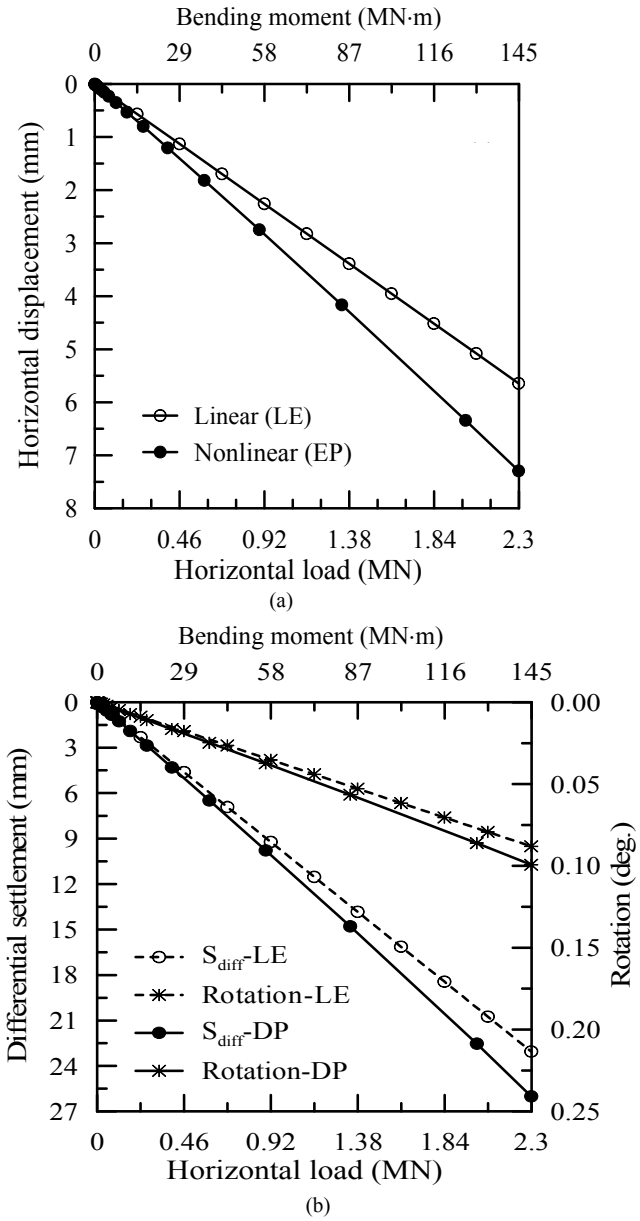

Fig. 8 (a) Horizontal displacement response and (b) differential settlement and rotation responses of the piled-raft foundation from ABAQUS

6. COMPARISON OF ANALYTICAL AND FINITE ELEMENT SIMULATION RESULTS

It was observed in the analytical design that the serviceability requirements control the final design of the piled-raft foundation. Hence, the serviceability requirements such as the vertical settlement, horizontal displacement, differential settlement, and the rotation of the piled-raft foundation for the design loads obtained from the analytical design method and finite element simulation were compared. In addition, the results obtained with the LE and DP soil models were compared. The comparison between them is presented in Table 3. In Table 3, the results for both linear and nonlinear soil models are presented for both methods. The

linear response for the vertical settlement obtained from the analytical method was determined by performing the vertical settlement analysis without hyperbolic factors, *i.e.,* entering $R_{fr} = R_{fp} = 0$ in Eq. (2) and the nonlinear response was obtained by entering $R_{fr} = 0.9$ and $R_{fp} = 0.2$ in Eq. (2). The analytical method presented in this study to calculate the differential settlement, rotation, and horizontal displacement do not consider the nonlinear soil response. Therefore, these values are not presented in Table 3. Further, the linear response from the finite element simulation was obtained by using the LE soil model and the nonlinear response was obtained by using the elastoplastic DP soil model. It should be noted that the vertical settlements for both methods shown in Table 3 are due to the vertical load only.

It was observed that the finite element simulation with the LE soil model under-predicts the vertical settlement by 43.33% and with the elastoplastic DP soil model under-predicts the vertical settlement by 43.19% compared to the analytical method. The horizontal displacement with the LE soil model was also underpredicted by the finite element model by 20.56%. On the other hand, the finite element predictions resulted in 118.48% and 350% higher differential settlement and rotation compared to the analytical results, respectively. It can be observed in Table 3 that the predictions with the LE soil model are always smaller than that of with the elastoplastic DP model.

Further, the vertical load-settlement responses obtained from the analytical (with and without hyperbolic factor) and finite element methods (with LE and DP soil models) at different vertical loads were compared and presented in Fig. 9. The same dimensions of the piled-raft foundation were used to perform this analysis. It can be observed that the vertical settlement obtained using the analytical method without the hyperbolic factor is lower compared to that obtained using the hyperbolic factor. However, the difference is almost negligible for lower vertical loads and increases with the increase in load. Moreover, it can also be observed that the vertical load-settlement curve from the analytical method without the hyperbolic factor is linear unlike the one with the hyperbolic factor which is nonlinear. Hence it can be concluded that the hyperbolic factor may be contributing to the nonlinear plastic deformation at the higher vertical loads. The vertical load-settlement curves obtained from the finite element simulation are also plotted in Fig. 9. It can be observed that while using the LE soil model, the finite element simulation resulted in a linear load-settlement curve while the use of the DP soil model resulted in a nonlinear response. When using the DP soil model, the gradient of the vertical-load settlement curve increased as the vertical load increased. As a result, the difference between the vertical settlements with the LE and DP model changes with the change in load. It can be seen in Fig. 9 that for lower loads (up to about 40 MN), the LE model result and DP model result is overlapping. This is because, at the lower loads, the LE and DP stress-strain relationship of soil overlaps as shown in Fig. 4(a). Moreover, the vertical settlement obtained from the finite element simulation is lower than the analytical solution for both the LE and DP soil models except for the vertical settlement at vertical loads higher than about 170 MN for the simulation with the DP soil model. For the vertical load higher than 170 MN, the vertical settlement obtained from the ABAQUS simulation with the DP soil model is higher than the analytical solution without the hyperbolic factor.

The comparison presented above is for the mean soil properties and load. To investigate the effect of variation in soil properties and loading and to calibrate the finite element model for a range of loading and soil strength and deformation, a parametric study was conducted by considering the variation in undrained cohesion and wind speed and presented in the next section.

Table 3 Comparison between the analytical method and FEM results

Method	Vertical settlement (mm)		Differential settlement (mm)		Rotation (°)		Horizontal displacement (mm)	
	Linear	Nonlinear	Linear	Non-linear	Linear	Non-linear	Linear	Non-linear
Analytical	40.00	44.78	10.55	-	0.04	-	7.10	-
ABAQUS	22.67	25.44	23.05	26.00	0.18	0.20	5.64	7.29
ABAQUS/Analytical	0.57	0.57	2.18	-	4.5	-	0.79	-

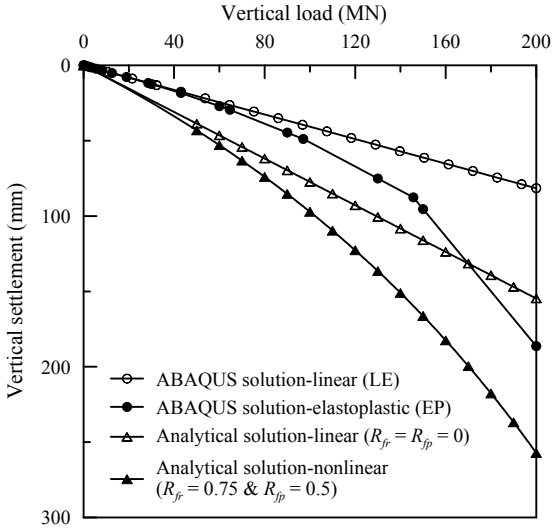

Fig. 9 Comparison of vertical load-settlement curve from analytical method and ABAQUS

6.1 Effect of Wind Speed and Undrained Cohesion on the Predicted Responses

The wind turbine is constructed in groups in a wind farm which extends over a large area. Hence, there will be a variation in soil strength parameter (undrained cohesion and corresponding modulus) and wind speed. The difference between the analytical result and the finite element simulation may not always be the same when the undrained cohesion and the wind speed change. Therefore, a parametric study was conducted to examine the effect of varying undrained cohesion and wind speed on the differential settlement over the wide range so that the accurate conclusion can be made. For this purpose, the mean design (length of pile, radius of raft, and number of piles) of piled-raft foundation for mean undrained cohesion and loading was used. The piled-raft foundation with the mean design was analyzed analytically and numerically for the range of undrained cohesion and wind speed. The undrained cohesion was varied between 40 kN/m^2 and 160 kN/m^2 at the interval of 20 kN/m^2 which fairly covers the clay with medium to very stiff consistency. Since the variation of the undrained cohesion affects the modulus of elasticity of the soil, the correlation between modulus of elasticity and the undrained cohesion obtained from the USACE (1990) was used to determine the corresponding modulus of elasticity for different undrained cohesion. Similarly, the wind speed was varied between 114.3 km/h and 288.2 km/h at the interval of 28.98 km/h. This range of wind speed covers the survival wind speed and all the category of hurricane. The corresponding design loads (horizontal load and bending moment) were calculated for each case of wind speed.

6.1.1 Effects of Undrained Cohesion on the Predicted Response

The piled-raft foundation designed considering the mean wind speed and undrained cohesion (N_p = 44, L_p = 28 m and R_r = 7.5 m) was used for investigating the effect of undrained cohesion. The finite element simulations were conducted by varying the undrained cohesion of the soil while keeping the wind speed at its mean value. The variation of the differential settlement obtained from the analytical method and the finite element method (with LE and DP soil models) are plotted in Fig. 10(a). The dispersion of the ratio of the differential settlement obtained from the finite element simulation and the analytical solution from the linear line ($x = y$ line) and the linear best fit line for the dispersion are plotted in Fig. 10(b). For the range of undrained cohesion considered, the differential settlement obtained from ABAQUS with the DP soil model was found to be higher than that obtained from ABAQUS with the LE soil model. However, the difference in the differential settlements obtained from the LE and DP soil models small when the undrained cohesion is between 120 kN/m^2 to 160 kN/m^2 . The difference seems to increase when the undrained cohesion is between 60 kN/m^2 to 120 kN/m^2. It can be seen in Figs. 10(a) and 10(b) that the differential settlement obtained from ABAQUS with LE and DP soil models is higher for the stronger/stiffer soil (c_u > 80 kN/m^2) than that of the analytical method. However, for the weaker/softer soil (c_u = 60 kN/m^2), the result was the opposite. From Fig. 10(b), it can be seen that the difference between the differential settlements obtained from the two methods increase when the undrained cohesion is decreasing from the highest value. But for the undrained cohesion of 60 kN/m^2, the opposite trend is observed (ABAQUS result < analytical solution) and the difference is smaller. This could be because for the undrained cohesion of 60 kN/m^2, the single pile capacity is reduced by 1.2 times compared to the capacity at 80 kN/m^2 that will result in significant reduction in capacity for the piled-raft in which there are 44 piles. This reduction in pile capacity results in a sudden increase in the differential settlement. Further, it can be noticed in Figs. 10(a) and 10(b) that the results for the undrained cohesion of 40 kN/m^2 is not present. This is because, while calculating the differential settlement using the analytical method, the settlement fell into the failure zone. As a result, it was not possible to calculate the differential settlement from the analytical method. Therefore, the differential settlement obtained from ABAQUS for the undrained cohesion of 40 kN/m^2 (which is 55.37 mm for LE model and 70.15 mm for DP model) was not presented as well.

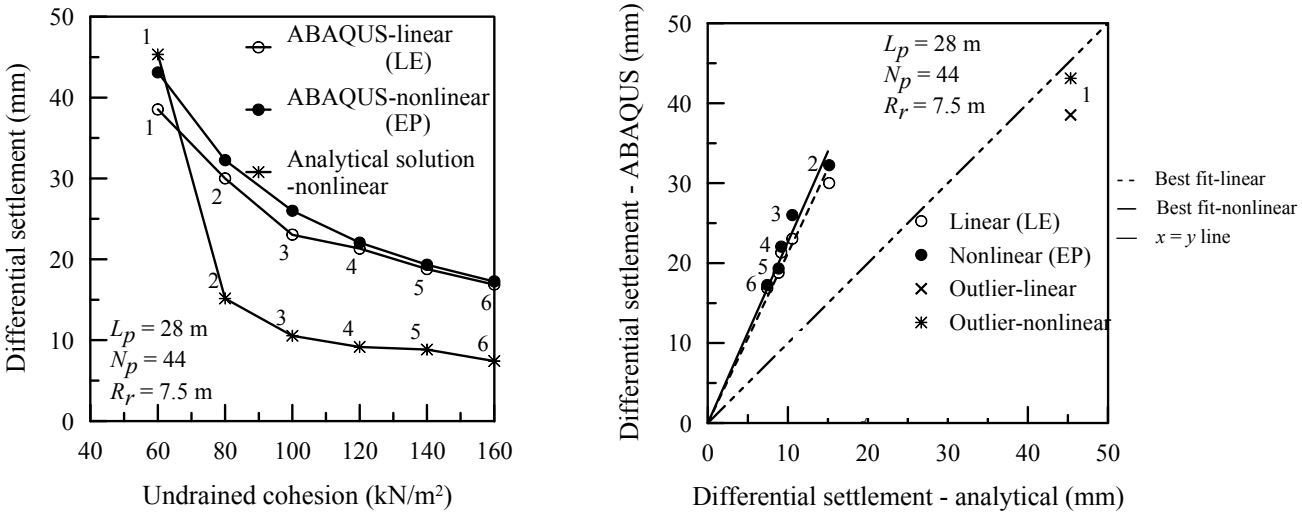

*Note: 1: 60 kN/m^2, 2: 80 kN/m^2, 3: 100 kN/m^2 (mean), 4: 120 kN/m^2, 5: 140 kN/m2, 6: 160 kN/m^2

(a) Comparison between analytical and ABAQUS results (b) Dispersion around Sdiff-analytical = Sdiff-ABAQUS line

Fig. 10 Effect of undrained cohesion on differential settlement

6.1.2 Effect of Wind Speed on the Predicted Response

The effects of variation in wind speed on the differential settlements obtained by keeping the undrained cohesion at its mean value from the analytical procedure and ABAQUS (with LE and DP soil models) are plotted in Fig. 11(a). From the figure, it is observed that the differential settlement is higher for the higher wind speed (*i.e.*, higher lateral loads) and lower for the lower wind speed. The dispersion of the ratio of the differential settlement obtained from the ABAQUS simulation and analytical method from the linear line ($x = y$ line) and the linear best fit line for the dispersion are plotted in Fig. 11(b). It can be observed in Fig. 11(a) that the differential settlements obtained from the finite element simulation by using the LE and DP soil models are nearly the same up to the wind speed of 143.3 km/h and the difference between them increases when the wind speed increases beyond 143.3 km/h. Further, the differential settlements obtained from the finite element simulation (both LE and DP soil models) for the range of wind speed considered in this study are always higher than that obtained from the analytical method. This observation is consistent with the previous parametric study in which the undrained cohesion was varied while keeping the wind speed at its mean value. However, the difference in the differential settlements obtained from the two methods is not always equal. With the increase in wind speed, the difference in the differential settlements obtained from the two methods slightly increased up to the wind speed of 230.23 km/h and then decreased when the wind speed increased from 230.23 km/h as can be observed in Fig. 11(a) and 11(b). At the wind speed of 259.2 km/h, the finite element simulation results with the LE soil model and analytical method converge. Moreover, a sudden increase in the differential settlement while increasing the wind speed from 230.2 km/h to 259.2 km/h for the analytical solution can also be observed. This could be because for the higher wind speed the load on the pile also increases but the soil strength remains the same. This results in an increase in differential settlement. It can be observed in Fig. 11 that the differential settlement for the highest wind speed of 288.2 km/h is not presented because similar to the case of the undrained cohesion variation, the analytical solution resulted in an unsafe design for the largest wind speed, *i.e.,* the settlement fell on the failure zone. Hence, it was not possible to calculate the differential settlement from the analytical method for the maximum wind speed. Therefore, the differential settlement obtained from the finite element simulation for the wind speed of 288.2 km/h (which is 50.96 mm for the LE model and 58.95 mm for the DP model) was not presented as well.

7. FURTHER INVESTIGATION OF PILED-RAFT FOUNDATION USING FINITE ELEMENT MODEL

The application of the computer software in the analysis of a complex problem has gained popularity with the development of the competent finite element program. For the complex problem in geotechnical engineering involving the soil-structure interaction and the combined loading like the one demonstrated in this study, an experimental analysis is challenging and expensive. A successful experimental study of a piled-raft-soil system under the application of the combined load needs careful pre-experiment planning and resources and yet the results may lack some data for analysis. In such a case, the experimental analysis may be expensive and impractical. An advanced validated/verified finite element model is a valuable tool. It can be used for gaining further insights that could not be possible or is expensive to obtain from an experimental method. The ABAQUS results for the mean design case was used for further investigating the behavior of the piled-raft foundation.

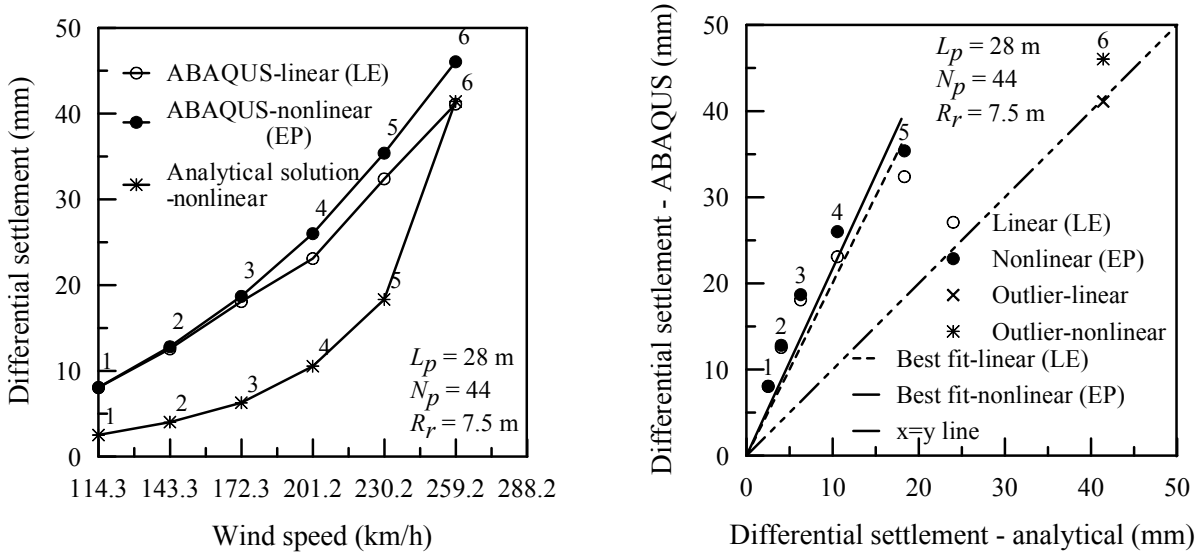

Note: 1: 114.3 km/h, 2: 143.3 km/h, 3: 172.3 km/h, 4: 201.3 km/h (mean), 5: 230.2 km/h, 6: 259.2 km/h

(a) Comparison between analytical and ABAQUS results (b) Dispersion around Sdiff-analytical = Sdiff-ABAQUS line

Fig. 11 Effect of wind speed on differential settlement

7.1 Behavior of Critical Piles

The piles in the piled-raft foundation under the bending moment are either in tension or in compression depending on the location of the piles and the direction of the moment. Among all the piles in the pile group, the piles located at the extreme edge of the raft along the direction of the bending moment are considered as critical piles in this study because they are under the highest tension or compression force and hence expected to have the minimum or the maximum settlement. The critical piles are shown in Fig. 12 where piles 1 and 2 are in compression and piles 3 and 4 are in tension.

7.1.1 Vertical Deformation of Critical Piles

In Fig. 12, the un-deformed shape and the vertical deformation of the piled-raft foundation (only critical piles) using DP soil model are shown. The other piles were removed for visualization of critical piles only. Figure 12 shows that the whole foundation has settled down vertically due to the vertical load and rotated due to the bending moment and horizontal load. A similar response was observed for the LE soil model which is not shown here.

The critical piles can either be compressed or elongated due to the combined action of vertical load, horizontal load and bending moment. To identify if a pile is compressed or elongated, the initial and final lengths of the pile are calculated based on the vertical coordinates of the pile top and tip at the end of the simulation and compared. The results of this analysis using both the LE and DP soil models are given in Table 4. It was found that the final lengths of all the critical piles under consideration are smaller than the initial length for both the LE and DP soil models. This indicates that these piles are in compression. The amount by which these piles have compressed are also tabulated in Table 4. It was found that for both the LE and DP soil models, pile no. 1 which is the farthest pile from the center of the foundation in the direction of the bending moment has the maximum compression. On the other hand, pile no. 4 which is the farthest pile from the center of the foundation opposite to the direction of the bending moment has the minimum compression. Further, piles no. 2 and 3 have the compression between the maximum and the minimum values. Hence it can be interpreted that the compression of all the other piles in between decrease from pile no. 1 to pile no. 4. Moreover, it can be observed that the use of DP soil model resulted in lower compression compared to the LE soil model. This result can be used to analyze the structural safety of the pile. For instance, it can be determined if the pile will still be intact when compressed or elongated by a certain amount.

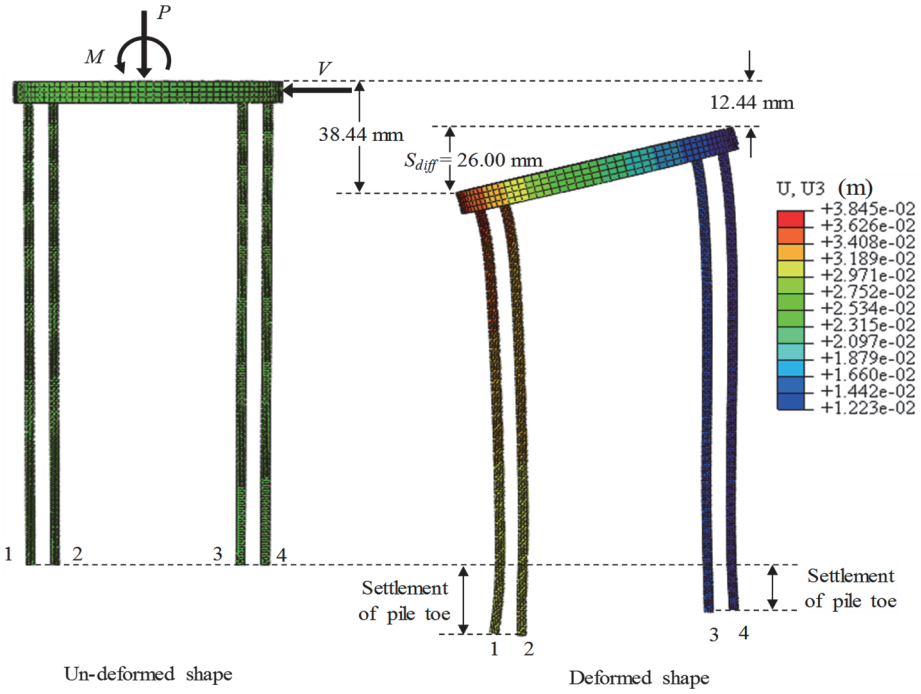

Fig. 12 Vertical deformation of the critical piles using DP soil model (other piles are removed for visualization purpose; deformation scale factor = 150)

Table 4 The final condition of critical piles

Pile no.*	Initial length (mm)	Linear elastic model		Drucker-Prager model	
		Final length (mm)	Compressed by (mm)	Final length (mm)	Compressed by (mm)
1	28000.0	27993.4	6.6	27993.62	6.38
2		27996.2	3.8	27996.35	3.65
3		27999.0	1.0	27999.16	0.84
4		27999.4	0.6	27999.68	0.32

Note: *Refer to Fig. 12 for pile no.

7.1.2 Separation and Slip Study between Soil and Pile

Furthermore, the separation and slip of the pile from the soil were also investigated. Since piles no. 1 and 4 have the maximum and the minimum settlement, respectively, they were taken as the sample to study the slip and separation at the soil-pile interface. Three locations were selected along the length of the pile to calculate the relative movement as shown in Fig. 13. These nodes lie on the cross-section of the pile. The common nodes to pile and soil are numbered from 1 to 8 on the left and 1′ to 8′ on the right at various locations along the length of pile. Nodes 1 to 3 and 1′ to 3′ are near the top of the pile, nodes 4 to 5 and 4′ to 5′ are around the middle of the pile, and nodes 6 to 8 and 6′ to 8′ are near the bottom of the pile.

The slip and separation were calculated as the difference between the initial and final coordinates in the vertical and horizontal directions, respectively. The separation and slip values calculated from the finite element simulation with the LE and DP soil models are presented in Table 5. Similar results were observed in both cases (LE and DP soil models) except for no slip at all on the right-side nodes while using the DP soil model. It was found that for pile no. 1 there is a separation and slip near the top on both sides (except node 3 and 1′ for LE model where no slip is observed) while middle section has no slip and separation except for node 5 with the LE soil model. Similarly, no slip was observed near the bottom of the piles except at node 6. While a separation of 0.01 mm was observed at nodes 6, 6′, and 7′ with the LE soil model and at node 7 with the DP soil model. For pile no. 4, a separation was observed at upper three nodes for both the LE and DP soil models and a slip was observed at nodes 1, 2, 3 with both the LE and DP soil models (except node 3 with DP soil model) and at node 1' with the LE soil model. For other nodes at the middle and bottom parts, the separation and slip were not observed except at nodes 6 and 6′ with the DP soil model where a negligible separation was observed. For both the piles, the maximum observed separation and slip is 0.02 mm for the LE soil model and 0.03 mm and 0.05 mm, respectively for the DP soil model. In summary, separation and slip were observed near the top of the pile while the bottom portion did not exhibit any separation or slip. The separation and slip have the tendency to decrease the pile capacity. Nevertheless, it can be predicted that there was no significant reduction in the pile capacity during the simulation because the separation and slip were negligible, and no unusual deformation was observed around the pile at the end of the simulation.

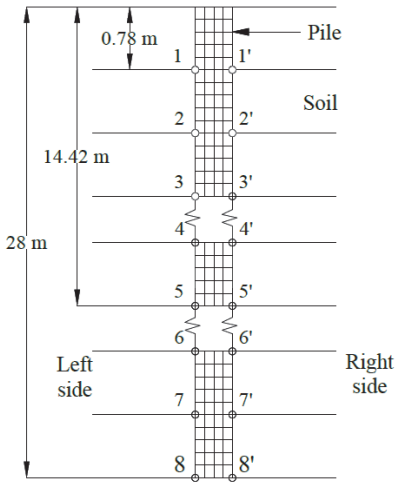

Fig. 13 Nodes defined for pile for slip and separation study

Table 5 Separation and slip of the critical piles (piles 1 and 4)

Pile no.*	Node**	Separation (mm)		Slip (mm)		Node**	Separation (mm)		Slip (mm)	
		LE	DP	LE	DP		LE	DP	LE	DP
1	1	0.02	0.03	0.01	0.05	1'	0.01	0.01	0	0
	2	0.02	0.02	0.01	0.01	2'	0.02	0.03	0.01	0
	3	0.01	0.01	0	0.01	3'	0.01	0.01	0.01	0
	4	0	0	0	0	4'	0	0	0	0
	5	0.01	0	0	0	5'	0	0	0	0
	6	0.01	0.01	0	0	6'	0.01	0.01	0	0
	7	0	0.01	0	0	7'	0.01	0.01	0	0
	8	0	0	0	0	8'	0	0	0	0
4	1	0.01	0.01	0.02	0.02	1'	0.02	0.01	0.01	0
	2	0.02	0.02	0.01	0.01	2'	0.01	0.01	0	0
	3	0.01	0.01	0.01	0	3'	0.01	0.01	0	0
	4	0	0	0	0	4'	0	0.01	0	0
	5	0	0	0	0	5'	0	0	0	0
	6	0	0.01	0	0	6'	0	0.01	0	0
	7	0	0	0	0	7'	0	0	0	0
	8	0	0	0	0	8'	0	0	0	0

Note: *Refer to Fig. 12 for pile no. **Refer to Fig. 13 for node no.

7.2 Surface Manifestation around the Foundation

Several views of the deformed shape of the piled-raft foundation and surrounding soil obtained from the finite element simulation with the elastoplastic constitutive model are shown in Fig. 14. From the figure, it can be seen that the system is settling down due to the vertical load and rotating due to lateral loads. A similar deformed shape was observed from the finite element simulation with the LE soil model which is not shown here.

7.3 Contribution of Raft and Piles in the Settlement Response of Piled-Raft Foundation

The major drawback in the currently available analytical design of the piled-raft foundation is that the load sharing between the raft and piles cannot be calculated. The determination of the load sharing between the raft and piles is complicated because the raft and pile capacities are mobilized at different settlements. The fact that the pile tip and pile head capacity are mobilized at different settlements, makes the determination of load sharing more complicated. If the load shared between the raft and piles was computable, then the raft and piles could be designed as a separate component to resist the shared load. This paper presents the use of validated sophisticated finite element model to determine the contribution of raft and piles in carrying the vertical load, horizontal load, and bending moment. To conduct this study, the computer models of pile group only and raft only with the same dimension as the mean design were created and then the vertical load up-to 150 MN, lateral load up-to 7 MN, and bending moment up-to 250 MNm were applied (one load at a time, not combined load). In the case with only piles, the pile head was fixed replicating the pile head connection. The piled-raft foundation was also subjected to the same loads (one load at a time). Then settlement responses (vertical, lateral, and differential settlements) of the individual components and the piled-raft foundation using LE and DP models were studied to understand the contribution of each component in the piled-raft foundation.

7.3.1 Vertical Load-Settlement Responses of Pile, Raft, and Piled-Raft

The vertical load-settlement responses of the three models (raft only, piles only, and piled-raft) obtained from ABAQUS using LE and DP soil models are plotted in Fig. 15. The foundations with LE model for soil resulted in a linear load-settlement response while the foundations with DP model for soil resulted in a nonlinear load-settlement response. In Fig. 15 (b), the load-settlement curve for the raft shows that the maximum vertical load is 90 MN. The curve was intentionally cut up to that point because the vertical settlement of the raft with DP soil model at 150 MN was computed to be 29,539.06 mm, which is extremely high to include in the plot. With no doubt, the vertical settlement obtained for the piled-raft foundation was the lowest of three cases for both LE and DP soil models followed by piles and raft foundation. The raft being load bearing component and the piles being settlement reducing component clearly justify why the raft resulted in higher settlement than the piles. At the vertical load of 90 MN, the vertical settlements observed in the pile-raft, piles, and raft using LE soil model were 36.69 mm

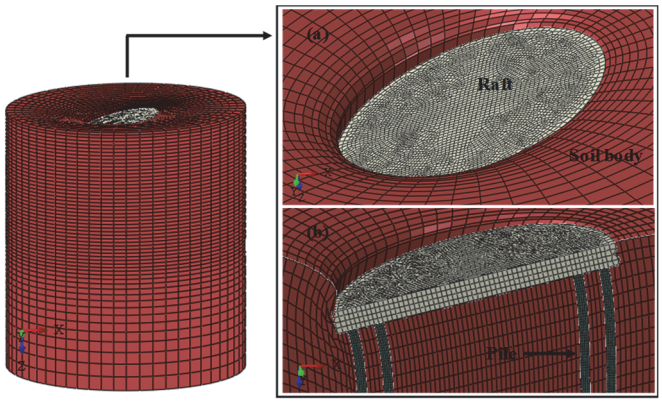

(a) Top view (b) Cross-section

Fig. 14 Surface manifestation at the ground surface for DP soil model

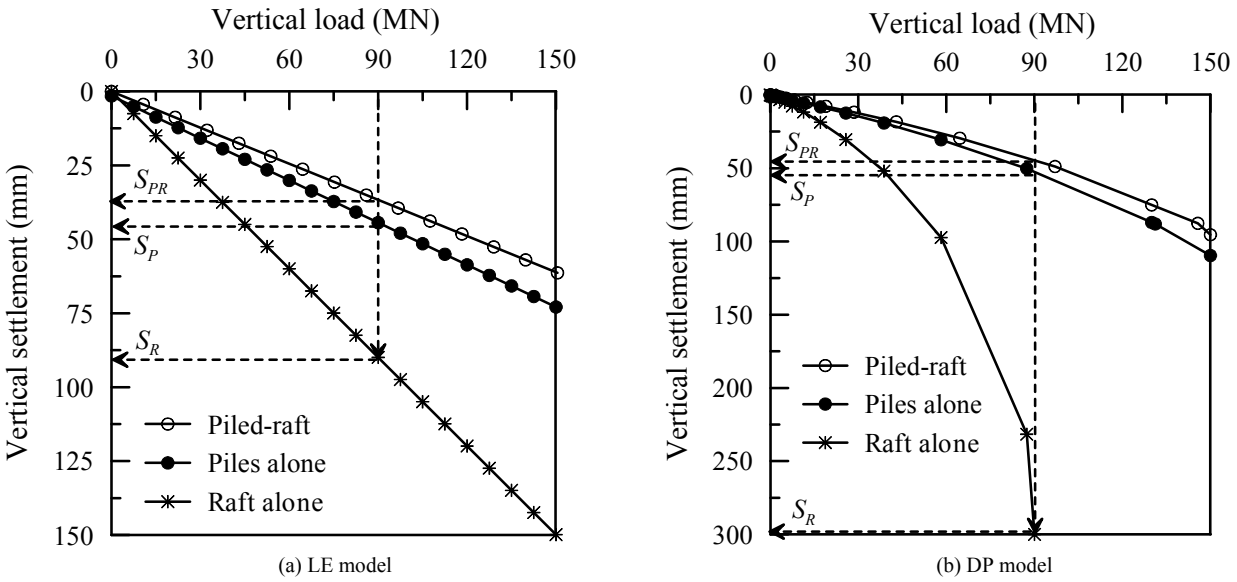

(a) LE model (b) DP model

Fig. 15 The vertical load-settlement responses of piled-raft, piles, and raft

(S_{PR}), 42.83 mm (S_P), and 89.93 mm (S_R), respectively as shown in Fig. 15(a). This indicates that the addition of raft to the piles contributed to the reduction of settlement by 14.4% while the addition of piles to the raft contributed to the reduction of settlement by 59.2%. This result is also true for other vertical loads shown in Fig. 15(a). On the other hand, at the same vertical load of 90 MN with DP soil model, the vertical settlements observed in piled-raft, piles, and raft were 44.64 mm, 52.45 mm, and 298.23 mm respectively. This indicates that while using DP constitutive model for soil, the addition of raft to the piles contributed to 14.89% reduction in the settlement while the addition of piles to the raft contributed in 85.03% reduction in the settlement. However, the percentage reduction in the settlement is not the same for other loads like in the case of LE soil model due to nonlinear load-settlement curve. By studying the result with both LE and DP soil models, it can be concluded that the piles have a higher contribution in reducing vertical settlement (also differential settlement) compared to the raft. The investigation of the deformed shapes of the three foundations at the end of vertical loading also did not show an unusual pattern.

7.3.2 Horizontal Load-Settlement/Displacement Responses of Pile, Raft, and Piled-Raft

The horizontal load-displacement responses of the three models (raft only, piles only, and piled-raft) obtained from ABAQUS using LE and DP soil models are plotted in Fig. 16(a) and 16(b), respectively. Similar to the vertical load-settlement plot, a linear load-settlement response was observed in the case of LE soil model and a nonlinear load-settlement response was observed in the case of DP soil model. It can be seen in Fig. 16 that the piled-raft foundation exhibited the lowest horizontal displacement followed by raft and piles foundations. At the horizontal load of 5 MN, the horizontal displacements observed in the piled-raft, piles, and raft were 5.30 mm ($S_{lat\text{-}PR}$), 6.62 mm ($S_{lat\text{-}P}$), and 5.98 mm ($S_{lat\text{-}R}$), respectively in the case of LE soil model. This indicates that the addition of raft to the piles contributed to 20% reduction in the horizontal displacement while the addition of piles to the raft contributed to 11.4% reduction in the horizontal displacement. This result is also true for other horizontal loads shown in Fig. 16. At the same horizontal load of 5 MN, the horizontal displacements observed in the piled-raft, piles, and raft while using the DP soil model were 5.77 mm, 6.87 mm, and 6.69 mm, respectively. This indicates that while using the DP soil model, the addition of raft to the piles resulted in 15.92% reduction in the horizontal displacement and the addition of piles to the raft resulted in 13.72% reduction. However, the percentage reduction in the horizontal displacement is not the same for other loads due to the nonlinear settlement curve. Thus, based on the observations of the results with the LE and DP constitutive models for the soil, it can be concluded that the raft has a higher contribution in reducing horizontal settlement compared to the piles.

7.3.3 Bending Moment-Differential Settlement Responses of Pile, Raft, and Piled-Raft

The bending moment-differential settlement responses of the three computer models of raft only, piles only, and piled-raft foundations with the LE and DP soil constitutive models are shown in Fig. 17(a) and 17(b), respectively. Similar to the previous load-settlement responses, a linear response is observed for this case as well while using the LE soil model and a nonlinear response is observed while using the elastoplastic DP soil model. In Fig. 17(b), the load-settlement curve for the raft shows that the maximum bending moment is 175 MNm. Similar to the case with vertical load, the curve was intentionally cut up to that point because the differential settlement of the raft with the DP soil model at 250 MNm was computed to be 599.97 mm, which is very high to include in the plot. The raft foundation is exhibiting the highest differential settlement of all the three foundations. It is interesting to observe that the differential settlement computed for the piled-raft foundation is slightly higher than the differential settlement computed for the piles only for both LE and DP soil model. This observation elucidates that the addition of raft to the piles is not contributing to reducing the differential settlement and piles are the only contributing factor in controlling the differential settlement in the piled-raft foundation. Nevertheless, it should be noted that the method of the application of bending moment may also affect the result. For instance, in the piled-raft

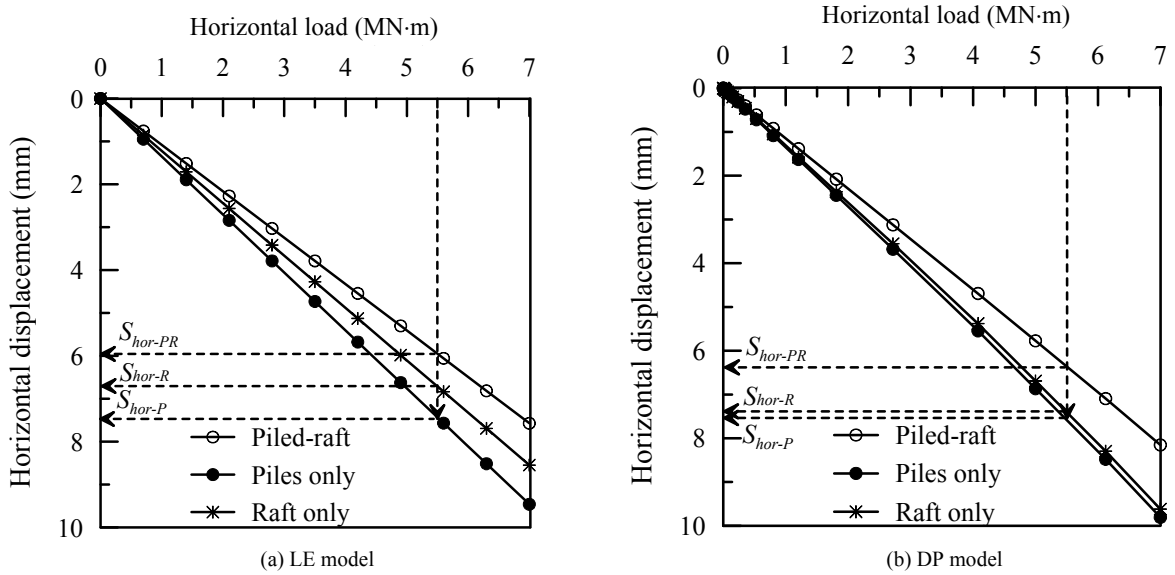

Fig. 16 The horizontal load-displacement responses of piled-raft, raft, and piles

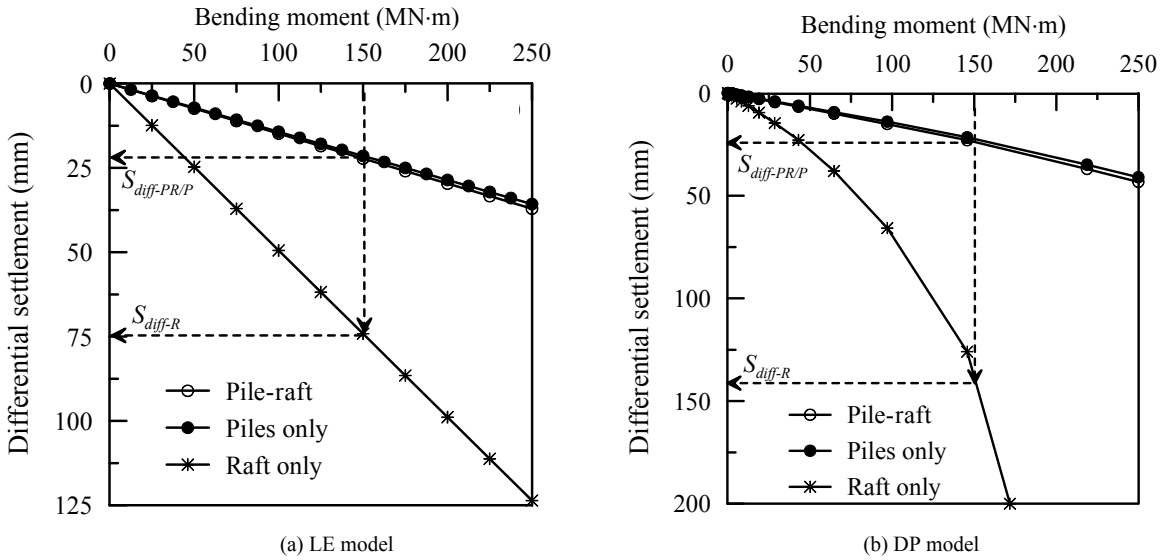

Fig. 17 The bending moment-differential settlement responses of piled-raft, raft, and piles

foundation, the bending moment was applied as a concentrated bending moment acting at the center of the raft which was transferred to the raft and piles by using the MPC bean constraint. While in the pile group, the vertical load induced due to the bending moment on each pile was calculated and applied as couples. These couple forces acting on the piles would provide the same bending moment. Further, in the case of piles only, the pile cap was not included while in the case of piled-raft foundation, the raft was included in the simulation. For a bending moment of 150 MNm, both the piled-raft and piles are exhibiting a differential settlement of about 22.30 mm ($S_{diff\text{-}PR/P}$) and the raft is exhibiting a differential settlement of 75 mm ($S_{diff\text{-}R}$) while using the LE soil model. In this case, the addition of the piles to the raft resulted in 70% reduction in the differential settlement which is also true for other load cases. At the same bending moment value, with DP soil model, both the piled-raft and piles are exhibiting a differential settlement of about 23.06 mm ($S_{diff\text{-}PR/P}$) and the raft is exhibiting a differential settlement of 138.16 mm ($S_{diff\text{-}R}$). In this case, the addition of piles to the raft resulted in 82.78% reduction in the differential settlement. However, unlike the case with LE soil model, the percentage reduction is not the same for the other load cases while using the DP soil model due to the nonlinear load-settlement curve.

8. CONCLUSIONS

In this study, a piled-raft foundation for a tall wind turbine tower in a clayey soil was designed using a simplified analytical method which showed that the differential settlement controlled the final design. The finite element analysis of the piled-raft foundation with both linear elastic (LE) and nonlinear elastoplastic Drucker-Prager (DP) constitutive models for the supporting soil was performed using ABAQUS. The comparison of the serviceability requirements obtained from the two methods for the mean loading and soil condition showed that the analytical method resulted in a higher vertical settlement and horizontal displacement compared to that obtained from ABAQUS with both the soil models. The differential settlement and rotation obtained from the analytical method were found to be lower than that of ABAQUS with both the soil models. Likewise, in the parametric study where the undrained cohesion of the soil and the wind speed were varied one at a time, the differential settlement obtained from the analytical solution was higher than that of finite element simulation with both LE and DP soil models. However, the result was opposite for the lower undrained cohesion (60 kN/m^2). For all the load cases, the finite element simulation with the DP soil model was predicting higher response compared to the LE soil model. The further investigation of the finite element analysis with the mean soil properties and load indicated that all the piles in the piled-raft foundation are under compression for both LE and DP soil models. The piled-raft foundation with DP soil model resulted in lower compression compared to the one with LE soil model. The amount by which the piles are compressed decreased from the extreme piles in the direction of the bending moment towards the piles in the opposite direction. Such a result can be used to perform the structural stability analysis of the piles. Moreover, it was found that there is insignificant to no slip and separation between the pile and soil with both soil models and hence it can be predicted that there was no significant decrease in pile capacity. Further, the deformation of the ground surface around the raft did not show any unusual behavior. The investigation of the vertical load carrying capacity of the individual components, *i.e.,* raft and piles showed that there is a higher contribution from piles in reducing the vertical settlement of the piled-raft foundation compared to the raft for both soil models. Similarly, it was found that the raft is contributing more in reducing the horizontal displacement of the piled-raft foundation for both soil models. Furthermore, it was found that only piles are contributing in controlling the differential settlement of the piled-raft foundation.

REFERENCES

ASCE (American Society of Civil Engineers). (2010). *Minimum Design Loads for Buildings and Other Structures*, Standard ASCE/SEI 7-10, ASCE, Reston, VA, USA, ISBN

978-0-7844-1085-1.

Burland, J.B. (1995). "Piles as settlement reducers." *18th Italian Congress on Soil Mechanics*, Keynote Address, Pavia, Italy.

Clancy, P. and Randolph, M. (1993). "Approximate analysis procedures for piled raft foundations." *International Journal for Numerical and Analytical Methods in Geomechanics*, **17** (12), 849 – 869. https://doi.org/10.1002/nag.1610171203

Fellenius, B.H. (1999). *Basics of Foundation Design*. 2nd Ed., BiTech Publishers, Richmond, British Columbia, ISBN: 978-1365824005.

Grunbeg, J. and Gohlmann, J. (2013). *Concrete Structures for Wind Turbines*. Wilhelm Ernst & Sohn, Berlin, Germany, ISBN 978-3-433-03041-7. http://doi.org/10.1002/9783433603291

Gudmundsdottir, B. (1981). *Laterally Loaded Piles*. M.S. Thesis, University of Alberta, Edmonton, Alberta, Canada.

Hemsley, J.A. (2000). *Design Applications of Raft Foundations*. Thomas Telford Ltd., Heron Quay, London, ISBN 0727727656. https://doi.org/10.1680/daorf.27657

Lee, J.H., Kim, Y., and Jeong, S. (2009). "Three-dimensional analysis of bearing behavior of piled raft on soft clay." *Computer and Geotechnics*, **37**(2010), 103–114. https://doi.org/10.1016/j.compgeo.2009.07.009.

Malhotra, S (2011). *Selection, Design and Construction of Offshore Wind Turbine Foundations, Wind Turbines*. Dr. Ibrahim Al-Bahadly, Ed., InTech, ISBN 978-953-307-221-0. https://doi.org/10.5772/15461.

Poulos, H.G. (2001). "Piled raft foundation: design and applications." *Geotechnique*, **51**(2), 95-113. https://doi.org/10.1680/geot.2001.51.2.95.

Poulos, H.G. and Bunce, G. (2008). "Foundation design for the Burj Dubai – The world's tallest building." *6th International Conference in Case Histories in Geotechnical Engineering*, Arlington, Virginia, USA.

Randolph, M.F. (1994). "Design methods for pile groups and piled rafts." *State-of-the-Arts Report, 13th International Conference on Soil Mechanics and Foundation Engineering*, New Delhi, India, **5**, 61-82.

Reul, O. and Randolph, M.F. (2003). "Piled rafts in overconsolidated clay: comparison of in situ measurements and numerical analyses." *Geotechnique*, **53**(3), 301-315. https://doi.org/10.1680/geot.2003.53.3.301.

Shrestha, S. and Ravichandran, N. (2016). "Design and analysis of foundations for onshore tall wind turbines." *Geo-Chicago 2016 GSP 270*, Chicago, IL, USA, 217-226. https://doi.org/10.1061/9780784480137.022.

Sinha, A. and Hanna, A.M. (2016). "3D numerical model for piled raft foundation." *International Journal of Geomechanics*, ASCE, **17**(2), 04016055, 1-9. https://doi.org/10.1061/(ASCE)GM.1943-5622.0000674.

Wagner, H.J. and Mathur, J. (2013). *Introduction to Wind Energy Systems: Basics, Technology and Operation*, 2nd Ed., Springer, Verlag Berlin Heidelburg, ISBN 9783642329753. https://doi.org/10.1007/978-3-642-32976-0.